Hindawi
Advances in Civil Engineering
Volume 2022, Article ID 9453702, 9 pages
https://doi.org/10.1155/2022/9453702

Research Article

Analysis of Mechanical Properties and Slope Stability of Red Bed Soft Rock: A Case Study in Xinjiang Irrigation Diversion Channel

Da Liu,[1] **Jianglin Gao**,[1] **Fang Chen**,[1] **Songtao Hu**,[1] **Xiaohua Zhao**,[2] **and Yan Li**[1]

[1]*Jiangxi Hydraulic Safety Engineering Technology Research Center, Jiangxi Academy of Water Science and Engineering, Nanchang 330029, China*
[2]*School of Water Conservancy Engineering, Zhengzhou University, Zhengzhou 450001, China*

Correspondence should be addressed to Fang Chen; jxgzld@126.com

Received 20 July 2022; Revised 4 September 2022; Accepted 6 September 2022; Published 16 November 2022

Academic Editor: Xiaobo Zhang

The channel slope in the red-bed soft rock area is prone to instability and collapse due to the influence of the channel flow movement, rainfall, weathering, and other factors. Under long-term operation conditions, the sediment stripped from the channel side wall is liable to silt along the process of water flow transportation in the channel, which seriously leads to elevation of the channel bottom, increase of channel width, and reduction of the horseway, which affect the normal water conveyance and operation safety of channels. In view of the collapse and instability of Zhetang diversion irrigation channel project in Xinjiang hydraulic project, through on-site sampling and indoor rock mechanics test, the strength mechanical parameters of slope rock samples are obtained, and the indoor rheological test is carried out, and the triaxial rheological law is obtained. Under different levels of stress, the axial creep strain accounts for more than 50% of the total axial strain, indicating that the rheological effect of sample rock is obvious. Based on the strength parameters of rock samples, a numerical model is established. The stability of red-bed soft rock channel bank slope is studied by using the strength reduction method of finite element method. The seepage field of channel slope under conventional working conditions is analyzed, and the slope stability under different operating conditions is compared and calculated. The results show that the slope stability safety factor of Zhetang diversion irrigation channel slope is 1.60 under conventional working conditions and 1.33 under check working conditions, which are greater than the recommended value in the specification.

1. Introduction

The red-bed soft rock slope is widely distributed in south China, which is easy to be weathered, disintegrated, and softened by water [1–3]. Most of the red-bed soft rocks can disintegrate into soil under open air or dry-wet cycle, and some even disintegrate immediately after immersion in water, or even muddy with poor engineering geological properties [4, 5]. Reservoirs and water diversion engineering channels are widely distributed and often need to run through the red-bed distribution area. The red-bed soft rock is prone to cracks, swelling, slope collapse, and other problems [6, 7], affecting the normal water delivery and operation safety of the water channel. Under long-term operation conditions, the sediment denuded from the channel sidewall is prone to siltation along the way through the flow transportation in the channel, which seriously leads to the elevation of the channel bottom, the increase of the channel width, and the reduction of the berm [8–10]. In addition, a large amount of sediment is brought into the reservoir by water flow, resulting in the deterioration of water quality in the reservoir area and affecting the storage capacity and service life of the reservoir [11, 12]. Therefore, it is urgent to study the seepage and stability of the red-bed soft rock channel bank slope, and reveal the mechanical mechanism, formation mechanism, and evolution law of the channel bank slope instability under the interaction of water and rock, and it is of great significance for the design and application of many channel slopes under construction or built [13].

Softening in water is an important factor that leads to the reduction of physical and mechanical properties of red-bed

soft rock, as a result, the rheological characteristics of soft rock under long-term load are important parameters for geotechnical engineering design [14–16]. The deformation and strength of soft rock have a strong time effect, which is reflected in many examples of rheology of soft rock caused by excavation in rock mass engineering such as dams, slopes, and caves. Shan et al. [17] analyzed the instantaneous strength and deformation characteristics of rock specimens by triaxial compression test and triaxial unloading creep test, and discussed creep deformation characteristics and damage evolution characteristics of red sandstone in concrete project, Yang et al. [18] analyzed the creep mechanical properties of red sandstone under different temperature and water content conditions. Yu et al. [19] carried out a series of uniaxial compressive strength tests and multistage creep tests on red sandstone samples to study the creep characteristics of red sandstone under different immersion conditions. In recent decades, based on various slopes, dams, and road projects, a large number of experiments have been carried out to study the rheological phenomena of soft rocks, and many rheological models have been put forward and established, including empirical formula model, unit model, and some new combined models formed by introducing damage mechanics and fracture theory [20–23]. Therefore, the creep characteristics of sandstone is of great significance for reasonably explaining the time-dependent mechanical behavior of slope engineering, and evaluating the long-term stability and safe operation of the project.

At present, the slope stability analysis methods are relatively mature, among which the most commonly used methods are limit equilibrium method and strength reduction method [24–26]. Limit equilibrium analysis method is a commonly used deterministic analysis method which is an earlier and widely used method in slope stability analysis [27, 28]. When using limit equilibrium method to analyze slope stability, the slope body is simplified, which is somewhat different from the real slope stress mode. Compared with the limit equilibrium method, the strength reduction method does not need assumptions, and can obtain the location of the sliding surface and the corresponding minimum safety factor according to the instability criterion, which makes it widely used. Arvin et al. [29] studied the three-dimensional stability of geocell reinforced slope by strength reduction method (SRM), which considered the geotechnical compartments and their fillers and surrounding soils. Zhang et al. [15] carried out numerical research on progressive failure process of jointed rock mass slope using fracture mechanics and strength reduction method (SRM), and proposed a displacement discontinuity method including friction unit for calculating stress intensity factor. Kong et al. [30] established a three-dimensional nonlinear strength model of soil considering the coupling strength of tension-shear (T-S) and compression-shear (C-S), and analyzed the stability of saturated and unsaturated slopes by strength reduction method.

Since the Zhetang diversion irrigation channel project was completed and put into operation, the red-bed slope of the channel often collapsed and cracked. For example, the slope collapse of the section with stake No. 1 + 650~2 + 300 was aggravated, and some of the slopes below the first-class Packway collapsed seriously. Therefore, in view of the collapse and instability of Zhetang diversion irrigation channel, and based on the indoor rock mechanics test and rock rheological test, the triaxial rheological law of channel rock samples are obtained. According to the obtained strength parameters of rock samples, a numerical calculation model is established, and the seepage and stability of red-bed soft rock channel slope are studied by using the strength reduction method, and the seepage field and stability safety factor of channel slope under conventional and check working conditions are analyzed.

2. Seepage and Stability Analysis Method

2.1. Seepage Analysis Method. The relationship between flow flux and soil and water potential gradient is often used to describe the movement law in unsaturated soil:

$$q = v = -k(\theta)\frac{\partial \psi}{\partial x}, \tag{1}$$

where q is the flow flux in unsaturated soil, v is the average flow rate, $\partial\psi/\partial x$ is hydraulic gradient.

The slope is assumed to be isotropic porous media, the seepage conforms to Darcy's law, and the motion equation of water in unsaturated soil:

$$\frac{\partial}{\partial x}\left(k_x\frac{\partial H}{\partial x}\right) + \frac{\partial}{\partial y}\left(k_y\frac{\partial H}{\partial y}\right) + Q = \frac{\partial \Theta}{\partial t}, \tag{2}$$

where H is the total head, k_x, k_y are the horizontal and vertical permeability coefficients, respectively, Q is the flow of water on the boundary, Θ is the volume moisture content.

The permeability law coefficient is defined as

$$\overline{k} = \frac{k_s}{\left(1 + \beta\sqrt{v_w v_w}\right)}k, \tag{3}$$

where $\overline{k}$ is the average permeability coefficient, k is the permeability coefficient of saturated soil, k_s is the seepage coefficient, β is a coefficient reflecting the influence of velocity on permeability coefficient, and v_w is the seepage velocity.

2.2. Strength Reduction Method. The strength reduction method defines the strength reduction factor as the ratio of the maximum shear strength that the slope can actually provide to the actual shear stress generated by the external load. Then, by continuously increasing the value of the reduction factor, repeatedly calculate and analyze until the value of the reduction factor increases to a certain value, the slope reaches the critical state, and calculate the cohesion and internal friction angle of rock and soil mass when the slope reaches the state of imminent failure [22]. In order to prevent the slope from losing stability at the beginning of the calculation and ensure the elastic state of the soil at the beginning stage, the initial value of F_t is usually taken as a number less than 1, and then gradually enlarged. This method has great advantages over traditional calculation

methods such as the slice method. It does not need to assume the shape and position of the sliding surface before calculation, and it can also observe the slope failure at different times.

The shear strength parameters after reduction can be expressed as

$$c_m = \frac{c}{F_t},$$
$$\varphi_m = \arctan\left(\frac{\tan\varphi}{F_t}\right), \tag{4}$$

where c_m and φ_m are the cohesion and internal friction angle that soil can provide, c and φ are the cohesion and internal friction angle required to maintain balance or actually exerted by the soil, F_t is the strength reduction factor.

3. Experimental Study on Mechanical Properties of Rock and Soil

3.1. Project Overview. Zhetang diversion irrigation channel of Xinjiang hydraulic project is located under the jurisdiction of Jizhou district and Jishui County of Ji'an city, which belongs to Wenshi River Basin, a tributary of Ganjiang River, and situated to typical red-bed soft rock in geological conditions. The Wenshi river originates from Dachong township, Ji'an County, and flows into the Ganjiang River at Jiangkou village under the well head through Yinwanqiao reservoir in Gujiang township. The total length of the Wenshi river is 48.1 km and the drainage area is about 360 km^2. After the construction of the protection zone, it is necessary to guide and drain the upstream water, with a rainwater collection area of 340.6 km^2, and a drainage and rainwater collection area of 19.4 km^2. In June 2021, the slope of Gushan section of the channel appeared local collapse, and then danger removal and reinforcement were carried out, as shown in Figure 1.

3.2. Triaxial Compression and Rheological Mechanical Properties. Rock samples taken on-site are conducted triaxial compression test by TAW-2000 microcomputer-controlled rock servo triaxial pressure testing machine, as shown in Figure 2. The sample is added indenters on both ends, sealed with sealing sleeves, installed with strain sensors, and put into the pressure chamber. The confining pressure is applied to the sample to reach the preset value, and the axial pressure is applied to the sample under the condition of keeping the confining pressure unchanged until the sample is destroyed. The confining pressure is set to three states, 1 MPa, 3 MPa, and 5 MPa are applied, respectively. According to the Mohr–Coulomb failure criterion, the shear strength parameters of the wet sample are calculated. The physical and mechanical parameters of the rock sample are summarized in Table 1.

Triaxial compression rheological tests were carried out on the rock samples. Based on the test results, the rheological properties of the rock were analyzed. Sr-6 triaxial creep instrument is used for rheological test, and the confining pressure of the test equipment uses air pressure as the pressure source. Through the pressure regulating valve, the stability of confining pressure during the test can be guaranteed. The test equipment can be controlled and automatically collect data through the software system, mainly including confining pressure, pore pressure, displacement, and deformation. The accuracy of deformation measurement is 0.01 mm. Gravity loading is adopted in axial stress loading, which can keep the axial pressure constant, and is the most commonly used loading method.

Considering the actual environmental conditions of the project, the drainage shear can more truly simulate the drainage conditions. The drainage shear is used in the test, and the test process is as follows:

(1) Sample preparation: The soil sampler is used for sample preparation, and the size is φ 61.8 × 123.6 mm cylindrical rock sample.

(2) Consolidation: 500 kPa confining pressure is used for drainage consolidation, and the consolidation time is 2-3 days. It is determined according to the dissipation of pore water pressure. In order to speed up the dissipation of pore water pressure and achieve more uniform consolidation, filter strips are uniformly pasted around the specimen along the axis. After consolidation, the consolidation deformation of the specimen is calculated based on displacement.

(3) Load: The test is carried out by using the step loading method. The loading time of each step depends on the deformation rate. Generally, if the total deformation is less than 0.01 mm within 3 days, it is considered that the creep is stable. When entering the lower-level loading, the applied stress levels are 0.4 MPa, 0.8 MPa, 1.2 MPa, and 1.6 MPa, respectively.

(4) Data collection: Record data every 30 seconds within 30 minutes after loading, and then record data every 1 minute.

Four levels of load were applied in the rheological test, and the duration of each level of load was more than 3000 minutes, with a total duration of 16330 minutes. Figure 3 shows the rheological curve of soft rock samples under graded loading. The value on the rheological curve represents the applied axial stress at all levels. Because the test adopts the graded loading method, it is necessary to use the Boltzmann superposition principle to process the test data, and transform the rheological curve in Figure 3 into the rheological curve of rock under different stress levels, as shown in Figure 3.

According to the test results, the instantaneous strain, creep strain, and total strain of rock axial under various stress levels are summarized in Table 2.

It can be seen from Figure 3 and Table 2 that the rheological curve reflects the first stage and the second stage of rheology, that is, the attenuation rheological stage and the stable rheological stage, but the third stage of rheology, that is, the accelerated rheological stage, was not observed in the test. The axial instantaneous strain, creep strain, and total

(a) (b)

Figure 1: Slope in Zhetang diversion irrigation channel. (a) Danger removal of Gushan section (in 2014 and 2019); (b) typical channel section on the left bank.

(a) (b)

Figure 2: Rock mechanics test. (a) Sample sampling; (b) TAW-2000 microcomputer-controlled rock servo triaxial pressure testing machine.

Table 1: Rock mechanics parameters.

Sample	Natural state			Shear strength		Permeability coefficient
	Water content W %	Wet density ρ g/cm^3	Dry density ρ_d g/cm^3	Cohesion c kPa	Friction angle φ °	K cm/s
ZT-1	24.5	1.95	1.57	27	18	7.0×10^{-6}

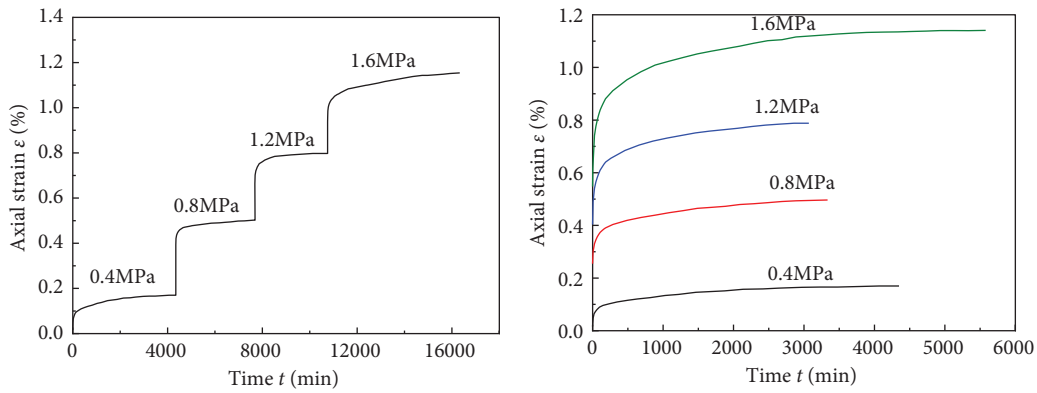

(a) (b)

Figure 3: Triaxial rheological mechanical property test. (a) Graded loading rheological curve; (b) axial loading rheological curve.

strain of the specimen increase with the increase of the stress level. Under all levels of stress, the proportion of axial creep strain to the total axial strain is more than 50%, indicating that the rheological effect of the specimen rock is obvious. Due to the weak argillaceous cementation between soft rock particles, large flow variables after rock saturation, and

Table 2: Axial instantaneous strain, creep strain, and total strain of rock under various stress levels.

$(\sigma_1$-$\sigma_3)$ (MPa)	Axial strain			
	Instantaneous strain (%)	Creep strain (%)	Total strain (%)	Creep strain/total strain (%)
0.4	0.0483	0.1358	0.1841	0.7378
0.8	0.2536	0.2569	0.5106	0.5032
1.2	0.3924	0.3999	0.7924	0.5047
1.6	0.5469	0.6080	1.1549	0.5264

Table 3: Physical and mechanical parameters of rock and soil mass.

Material	Density (kg/m^3)	Modulus of elasticity (GPa)	Poisson's ratio	Internal friction angle (°)	Cohesion (kPa)
Red-bed soft rock	1920	0.70	0.30	18.0	27.0
Weak interlayer	1840	0.50	0.33	9.5	10.0
Weakly weathered bedrock	2300	1.50	0.265	35.0	100.0

significant aging deformation, the rheological mechanical properties of rock have a great impact on the long-term stability and safe operation of the diversion project.

4. Slope Seepage and Stability Analysis

4.1. Calculation Model and Parameters. Taking Zhetang channel in Xinjiang reservoir area as the analysis object, the finite element analysis model of the channel is established, which is based on the design drawings and field survey, as shown in Figure 1. The channel model is divided into three levels of slope step on the right bank red layer soft rock slope, with the elevation of channel bottom 44.0 m and the width of slope step 3 m, in which the ratio of the first stage slope to the second stage is 1 : 2.0. The third and the fourth stage slope ratio is 1 : 1.5. The slope ratio of the first and second stage of the left bank is 1 : 2.0 and 1 : 1.5, respectively. The values of physical and mechanical parameters of rock and soil mass used in the calculation are shown in Table 3.

The calculation is divided into two working conditions, namely, conventional and check working condition. Because the rock mass strength of the weak interlayer has significant strain softening characteristics, a large number of projects show that the occurrence of landslide is often related to the penetrating weak interlayer. Therefore, in order to observe and verify the stability of the channel slope containing the weak interlayer, the dangerous working conditions containing the deep penetrating weak interlayer are set to verify the stability and safety of the channel slope, as shown in Figure 4. The physical and mechanical parameters of common soft interbeds in red beds are shown in Table 4.

Mohr–Coulomb criterion of elastic-plastic model is adopted in the constitutive model of material calculation simulating rock and soil mass, and its yield function is

$$F = \frac{1}{3} I_1 \sin\varphi + \left(\cos\theta_\sigma - \frac{1}{\sqrt{3}} \sin\theta_\sigma \sin\varphi \right) \sqrt{J_2} - \cos\varphi = 0, \tag{5}$$

where $I_1 = \sigma_x + \sigma_y + \sigma_z$ is the first stress invariant, θ_σ is the lode angle, $-30^\circ \le \theta_\sigma \le 30^\circ$, and $J_2 = 1/6[(\sigma_x - \sigma_y)^2 + (\sigma_y - \sigma_z)^2 + (\sigma_z - \sigma_x)^2] + \tau_{xy}^2$ is the second invariant of stress bias.

4.2. Seepage Analysis. The steady-state seepage analysis of the channel slope is carried out to analyze the seepage field of the channel slope. On the basis of the steady-state seepage, the rainfall infiltration analysis is added. Assuming that the rainfall infiltration intensity is $i = 0.02$ m/h, the slope infiltration intensity is corrected according to the slope, and the following formula is used for calculation:

$$i_\theta = i \times \cos\theta, \tag{6}$$

where i_θ is the infiltration intensity of slope surface and θ is the angle between slope and horizontal plane.

According to the pore water pressure nephogram in Figure 5, with the increase of depth, the pore pressure increases, and the maximum pore pressure is about 200 kPa. The upper part of the slope is unsaturated soil. With the gradual decrease of saturation, the greater the matrix suction, and the maximum matrix suction is about −200 kPa. The influence of rainfall on pore water pressure shown in Figure 6 is mainly reflected in the shallow surface, the pore water pressure on the top of the slope decreases, and the pore water pressure on the bottom of the slope almost remains unchanged.

4.3. Slope Stability Analysis. The slope stability calculation process is divided into two steps. The first step is the steady-state seepage, and the second step is to determine the safety factor of the slope in the critical instability state by reducing the strength factor of the channel slope under the initial equilibrium conditions calculated in the first step.

4.3.1. Conventional Working Conditions. The equivalent plastic strain nephogram and cumulative plastic strain nephogram when reduced to the critical state are shown in Figure 7. By observing that in the process of soil strength reduction, the plastic deformation develops until penetration, and the soil on the sliding surface appears plastic flow, resulting in the instability of the slope along the sliding surface, and the most dangerous arc surface of the channel slope under the critical value of strength reduction can be visually observed.

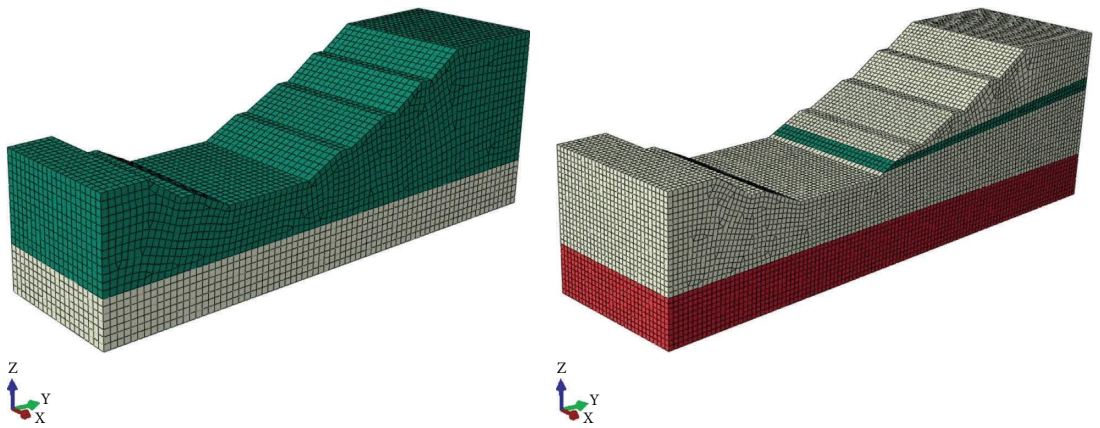

(a) (b)

Figure 4: Numerical calculation model of Zhetang slope. (a) Conventional working condition; (b) check working condition.

Table 4: Mechanical properties of common structural planes of red-bed soft rock.

Rock	Structural plane type	Cohesion (kPa)	Friction angle (°)
Mudstone	—	0.06–0.08	20–30
Siltstone	—	0.03–0.25	20–50
Sandstone	—	0.07–1.0	15–60
—	Pure mud type	2–5	10–14
—	Mud debris type	20–50	14–19
—	Debris mud type	50–100	19–22
—	Rock fragment type	100–250	22–29
—	Closed structural plane	50–150	22–35

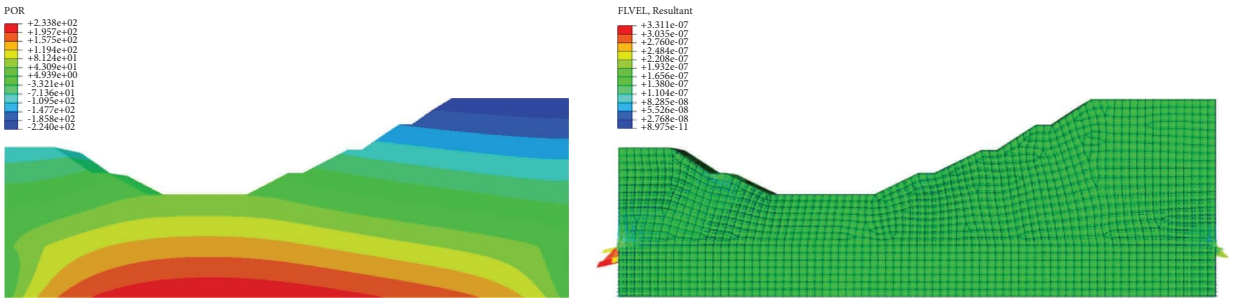

(a) (b)

Figure 5: Seepage analysis of steady channel slope. (a) Pore water pressure nephogram; (b) flow field distribution.

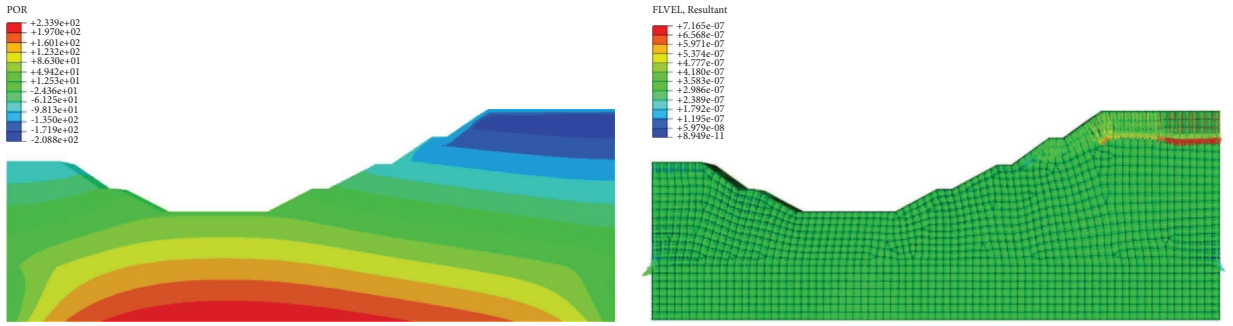

(a) (b)

Figure 6: Seepage analysis under the influence of rainfall. (a) Pore water pressure nephogram; (b) flow field distribution.

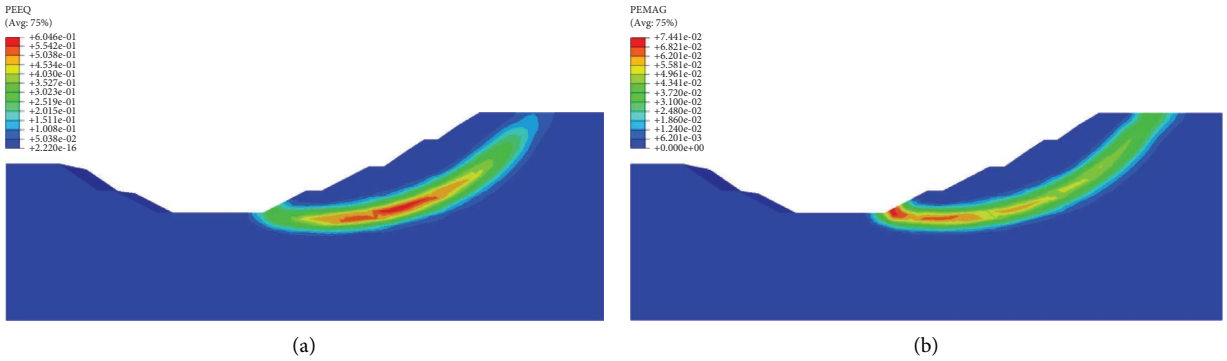

Figure 7: The most dangerous sliding surface under conventional working conditions. (a) Equivalent plastic strain nephogram; (b) cumulative plastic strain nephogram.

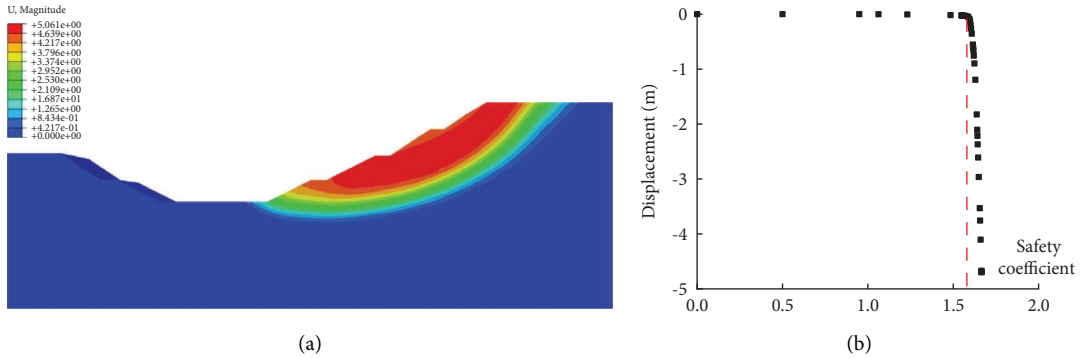

Figure 8: Displacement and safety factor under conventional working conditions. (a) Displacement nephogram; (b) stability safety factor.

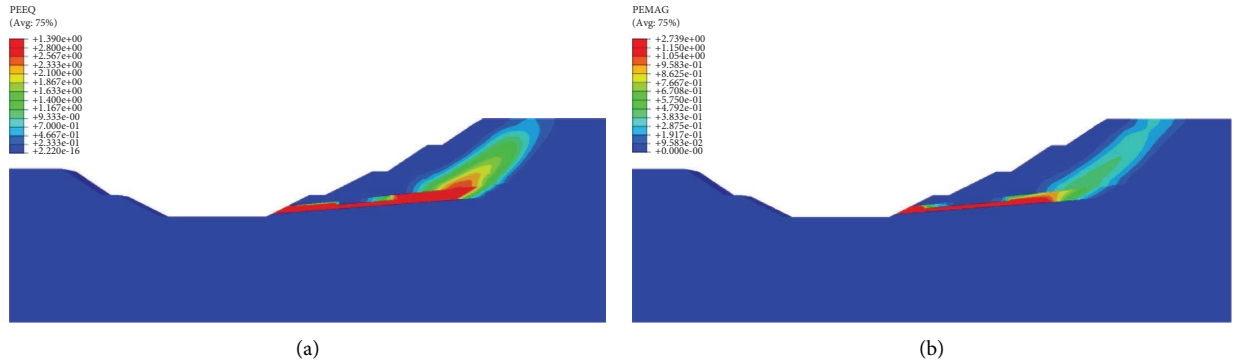

Figure 9: The most dangerous sliding surface under check condition. (a) Equivalent plastic strain nephogram; (b) cumulative plastic strain nephogram.

The relationship between the stability safety factor F_t and displacement at the starting point of the slope top slip arc is shown in Figure 8. With the increase of F_t, the plastic region in the slope rock mass gradually increases. A large number of practices have proved that the slope instability can be identified by observing the inflection point of displacement change mutation at the top of the slope. The analysis process of this method is similar to the slope failure process, and it also has clear physical significance. As can be seen from Figure 8(b), when the on-site variable changes to 1.59–1.62, displacement rapidly increases from 0.05 m to 0.76 m, which shows that the safety factor of slope stability in this critical state is about 1.60.

4.3.2. Check Condition. The equivalent plastic strain nephogram and cumulative plastic strain nephogram reduced to the critical state are shown in Figure 9, which can visually observe the most dangerous arc surface of the channel slope under the condition of the critical value of strength reduction. Due to the existence of deep through weak interlayer, the landslide surface is more inclined to slide along the tendency of the soft interlayer along the slope.

Figure 10 shows the relationship between the stability safety factor F_t and displacement at the starting point of the slope top slip arc under check condition, in which the slope rock mass tends to slide along the weak interlayer. When the

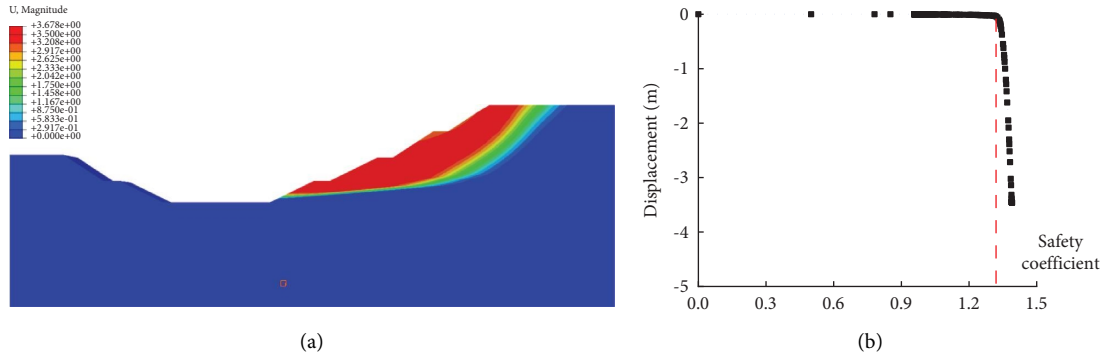

Figure 10: Displacement and safety factor under check condition. (a) Displacement nephogram; (b) stability safety factor.

on-site variable changes to 1.29–1.35, displacement rises rapidly from 0.02 m to 0.38 m, and the slope stability safety factor under this critical state is about 1.33.

The stability safety factor of the conventional working condition is greater than that of the check working condition. The occurrence of deep penetrating weak interlayer will induce the slope slip surface to the weak interlayer surface, and aggravate the risk of instability and failure of the channel slope.

5. Conclusion

Aiming at the channel slope project in Zhetang protection area of Xinjiang reservoir protection project, this study adopts the method of combining indoor geotechnical mechanical test and numerical calculation and carries out the stability analysis of the channel slope based on the finite element strength reduction method. The following conclusions can be drawn:

(1) Through the test of rock and soil mechanical properties, the strength mechanical properties parameters of the slope rock samples are obtained, and the triaxial rheological law are obtained. The axial instantaneous strain, creep strain, and total strain of the samples increase with the increase of the stress level. At all levels of stress, the proportion of axial creep strain to the total axial strain is more than 50%, indicating that the rheological effect of the sample rock is obvious.

(2) With the increase of depth, pore water pressure increases and matrix suction decreases. The influence of rainfall on pore water pressure is mainly reflected in the shallow surface, the pore water pressure on the top of the slope decreases, and the pore water pressure on the bottom of the slope almost remains unchanged.

(3) The existence of weak interlayer and structural plane will make the slope sliding surface concentrate to the weak surface, reduce the stability safety factor, and aggravate the risk of instability and failure of the channel slope.

(4) Based on results obtained by geotechnical test and numerical analysis, the safety factor of slope stability under conventional and check working conditions of Zhetang channel slope is 1.60 and 1.33, respectively. The safety factor of both conventional and check working conditions is greater than the recommended value of the specification, and the channel slope is generally safe and stable. The local collapse of channel slope is mostly caused by the decline of loose rock and soil mass on the slope, which may be induced by the weathering, disintegration, and creep of red-bed soft rock.

Data Availability

The data that support the findings of this study are available from the corresponding author upon reasonable request.

Conflicts of Interest

The authors declare that they have no conflicts of interest.

Acknowledgments

This work is supported by Jiangxi Provincial Natural Science Foundation (20212BAB214044 and 20204BCJ23002), and supported by the National Natural Science Foundation of China (51779190, 51779193, and 52009126), and Jiangxi Provincial Department of Water Resources Foundation (202224ZDKT08). The authors wish to express their thanks to all supporters.

References

[1] Z. T. Zhang, W. H. Gao, C. F. Zeng, X. Y. Tang, and J. Wu, "Evolution of the disintegration breakage of red-bed soft rock using a logistic regression model," *Transportation Geotechnics*, vol. 24, Article ID 100382, 2020.

[2] K. Huang, B. Kang, F. Zha, Y. Li, Q. Zhang, and C. Chu, "Disintegration characteristics and mechanism of red-bed argillaceous siltstone under drying–wetting cycle," *Environmental Earth Sciences*, vol. 81, no. 12, p. 336, 2022.

[3] C. Xia, C. Zhou, F. Zhu, Z. Liu, and G. Cui, "The critical indicator of red-bed soft rocks in deterioration process induced by water basing on renormalization group theory," *Applied Sciences*, vol. 11, no. 17, p. 7968, 2021.

[4] T. Wen, H. Tang, Y. Wang, J. Ma, and Z. Fan, "Mechanical characteristics and energy evolution laws for red bed rock of

badong formation under different stress paths," *Advances in Civil Engineering*, vol. 2019, Article ID 8529329, 16 pages, 2019.

[5] Z. Miao, P. Tang, and Y. Zhang, "Recognition of red-bed landslides over eastern sichuan through remote sensing and field investigations," *Geofluids*, vol. 2022, Article ID 9385352, 9 pages, 2022.

[6] Z. Zhang, X. Fu, Q. Sheng, D. Yin, Y. Zhou, and J. Huang, "Effect of rainfall pattern and crack on the stability of a red bed slope: a case study in yunnan province," *Advances in Civil Engineering*, vol. 2021, Article ID 6658211, 2021.

[7] Z. Liu, X. He, J. Fan, and C. Zhou, "Study on the softening mechanism and control of red-bed soft rock under seawater conditions," *Journal of Marine Science and Engineering*, vol. 7, no. 7, p. 235, 2019.

[8] H. Liu, D. Ma, C. Wang, X. Liu, D. Wu, and K. U. J. Khan, "Study on the frost heave mechanism of the water conveyance canal and optimized design of slope protection," *Bulletin of Engineering Geology and the Environment*, vol. 80, no. 11, pp. 8397–8417, 2021.

[9] C. Zhang, Zy Cai, Yh Huang, and H. Chen, "Laboratory and centrifuge model tests on influence of swelling rock with drying-wetting cycles on stability of canal slope," *Advances in Civil Engineering*, vol. 2018, Article ID 4785960, 10 pages, 2018.

[10] I. Abd-Elaty, H. Eldeeb, Z. Vranayova, and M. Zelenakova, "Stability of irrigation canal slopes considering the sea level rise and dynamic changes: case study el-salam canal, Egypt," *Water*, vol. 11, no. 5, p. 1046, 2019.

[11] P. Jamsawang, P. Boathong, W. Mairaing, and P. Jongpradist, "Undrained creep failure of a drainage canal slope stabilized with deep cement mixing columns," *Landslides*, vol. 13, no. 5, pp. 939–955, 2016.

[12] H. x. Chu, S. Mei, Xh Gao, Zh Fang, and J. Feng, "Analysis of formation and slope stability in caofeidian channel in bohai bay," *China Geology*, vol. 2, no. 2, pp. 189–197, 2019.

[13] S. Liu, Y. Lu, L. Weng, and F. Bai, "Field study of treatment for expansive soil/rock channel slope with soilbags," *Geotextiles and Geomembranes*, vol. 43, no. 4, pp. 283–292, 2015.

[14] S. Guo, S. Wen, H. Guo, and H. Fu, "The creep test study and macro-detail analysis of argillaceous red sandstone in different water-containing states," *Advances in Civil Engineering*, vol. 2022, Article ID 9698675, 8 pages, 2022.

[15] K. Zhang, P. Cao, J. Meng, K. Li, and W. Fan, "Modeling the progressive failure of jointed rock slope using fracture mechanics and the strength reduction method," *Rock Mechanics and Rock Engineering*, vol. 48, no. 2, pp. 771–785, 2015.

[16] G. Liu, X. Huang, and J. Pang, "The uniaxial creep characteristics of red sandstone under dry-wet cycles," *Advances in Civil Engineering*, vol. 2020, Article ID 8841773, 13 pages, 2020.

[17] R. l. Shan, Y. Bai, Y. Ju, Ty Han, Hy Dou, and Zl Li, "Study on the triaxial unloading creep mechanical properties and damage constitutive model of red sandstone containing a single ice-filled flaw," *Rock Mechanics and Rock Engineering*, vol. 54, no. 2, pp. 833–855, 2021.

[18] X. Yang, A. Jiang, and X. Guo, "Effects of water content and temperature on creep properties of frozen red sandstone: an experimental study," *Bulletin of Engineering Geology and the Environment*, vol. 81, no. 1, p. 51, 2021.

[19] C. Yu, S. Tang, C. Tang et al., "The effect of water on the creep behavior of red sandstone," *Engineering Geology*, vol. 253, pp. 64–74, 2019.

[20] Y. Song, Y. Che, L. Zhang, J. Ren, S. Chen, and M. Hu, "Triaxial creep behavior of red sandstone in freeze-thaw environments," *Geofluids*, vol. 2020, Article ID 6641377, 20 pages, 2020.

[21] D. Wang, G. Chen, D. Jian, J. Zhu, and Z. Lin, "Shear creep behavior of red sandstone after freeze-thaw cycles considering different temperature ranges," *Bulletin of Engineering Geology and the Environment*, vol. 80, no. 3, pp. 2349–2366, 2021.

[22] Y. Song, L. Zhang, H. Yang, J. Ren, and Y. Che, "Experimental study on the creep behavior of red sandstone under low temperatures," *Advances in Civil Engineering*, vol. 2019, Article ID 2328065, 9 pages, 2019.

[23] S. Q. Yang and B. Hu, "Creep and long-term permeability of a red sandstone subjected to cyclic loading after thermal treatments," *Rock Mechanics and Rock Engineering*, vol. 51, no. 10, pp. 2981–3004, 2018.

[24] B. S. Firincioglu and M. Ercanoglu, "Insights and perspectives into the limit equilibrium method from 2D and 3D analyses," *Engineering Geology*, vol. 281, Article ID 105968, 2021.

[25] A. Kaur and R. K. Sharma, "Slope stability analysis techniques: a review," *International Journal of Engineering Applied Sciences and Technology*, vol. 1, no. 4, pp. 52–57, 2016.

[26] S. M. Seyed-Kolbadi, J. Sadoghi-Yazdi, and M. A. Hariri-Ardebili, "An improved strength reduction-based slope stability analysis," *Geosciences*, vol. 9, no. 1, p. 55, 2019.

[27] S. Liu, Z. Su, M. Li, and L. Shao, "Slope stability analysis using elastic finite element stress fields," *Engineering Geology*, vol. 273, Article ID 105673, 2020.

[28] D. Dong-ping, L. Liang, W. Jian-feng, and Z. Lian-heng, "Limit equilibrium method for rock slope stability analysis by using the Generalized Hoek–Brown criterion," *International Journal of Rock Mechanics and Mining Sciences*, vol. 89, pp. 176–184, 2016.

[29] M. R. Arvin, A. Zakeri, and M. Bahmani Shoorijeh, "Using finite element strength reduction method for stability analysis of geocell-reinforced slopes," *Geotechnical & Geological Engineering*, vol. 37, no. 3, pp. 1453–1467, 2019.

[30] X. Kong, G. Cai, Y. Cheng, and C. Zhao, "Numerical implementation of three-dimensional nonlinear strength model of soil and its application in slope stability analysis," *Sustainability*, vol. 14, no. 9, p. 5127, 2022.